# Extracellular vesicle-mediated release of bis(monoacylglycerol)phosphate is regulated by LRRK2 and Glucocerebrosidase activity

Elsa Meneses-Salas[1], Marianna Arnold[2,#], Moises Castellá[1,#], Frank Hsieh[2], Ruben Fernández-Santiago[3,4], Mario Ezquerra[3,4], Alicia Garrido[3,4], María-José Martí[3,4], Carlos Enric[1], Suzanne R. Pfeffer[5], Kalpana Merchant[6,*] and Albert Lu[1*]

[1]Departament de Biomedicina, Unitat de Biologia Cel·lular, Facultat de Medicina i Ciències de la Salut, Centre de Recerca Biomèdica CELLEX, Institut d'Investigacions Biomèdiques August Pi i Sunyer, Universitat de Barcelona, Barcelona, Spain.

[2]NextCea Inc., Woburn, MA, USA

[3]Lab of Parkinson Disease and Other Neurodegenerative Movement Disorders, Institut d'Investigacions Biomèdiques August Pi i Sunyer (IDIBAPS), Institut de Neurociències, Universitat de Barcelona, ES-08036, Barcelona, Spain.

[4]Parkinson Disease and Movement Disorders Unit, Neurology Service, Institut Clínic de Neurociències, Hospital Clínic de Barcelona, ES-08036, Barcelona, Spain.

[5]Department of Biochemistry, Stanford University, Stanford CA, USA 94305-5307

[6]Department of Neurology, Northwestern University, Chicago, IL, USA

[#]These authors contributed equally to this work

[*]To whom correspondence should be addressed. E-mail:
albertlu@ub.edu or
kalpana.merchant@northwestern.edu

**Albert Lu Address:**
C/ Casanova 143
08036 Barcelona
SPAIN
**phone:** +34 93 227 5400 ext. 3358 / **FAX:** +34 93 402 1907

**RELEVANT CONFLICTS OF INTEREST/FINANCIAL DISCLOSURES:** Dr. Hsieh and Ms. Arnold are employed by Nextcea, Inc., which holds patent rights to the di-22:6-BMP and 2,20-di-22:6-BMP biomarkers for neurological diseases involving lysosomal dysfunction (US 8,313,949, Japan 5,702,363, and Europe EP2419742).

**FUNDING AGENCIES:** This research was funded by the Michael J. Fox Foundation (MJFF-019043).

**KEYWORDS:**

Parkinson's disease; bis(monoacyglycerol)phosphate; Endo-lysosomes; Extracellular vesicles; Exosomes

**ABBREVIATIONS:**

BMP, bis(monoacyglycerol)phosphate; CBE, conduritol b-epoxide; DHA, docosahexaenoic acid; GCase, glucocerebrosidase; ILV, intralumenal vesicle; LBPA, Lysobisphosphatidic acid; LRRK2, leucine-rich repeat kinase 2; PD, Parkinson's disease; WT, wild type

**ABSTRACT**

The endo-lysosomal phospholipid, bis(monoacylglycerol)phosphate (BMP), is aberrantly elevated in the urine of Parkinson's patients with mutations in genes encoding leucine-rich repeat kinase 2 (LRRK2) and glucocerebrosidase (GCase). Because BMP resides on and regulates the biogenesis of endo-lysosomal intralumenal membranes that become extracellular vesicles (EVs) upon release, we hypothesized that elevated urinary BMP may be driven by increased exocytosis of BMP-enriched EVs. To test this hypothesis, we analyzed BMP metabolism and EV-associated release of BMP in wild type (WT) and R1441G LRRK2-expressing mouse embryonic fibroblast (MEF) cells. Using immunofluorescence microscopy and transmission electron microscopy we detected structural alterations in endo-lysosomes and antibody-accessible BMP pool, indicating that mutant LRRK2 affects endolysosomal homeostasis. Biochemical analyses of isolated EV fractions confirmed the effect on endo-lysosomes by showing an increase in LAMP2-positive EVs in mutant cells, which was partially restored by LRRK2 kinase inhibition but further augmented by GCase inhibition. Using mass spectrometry, we detected an overall increase in total di-22:6-BMP and total di-18:1-BMP in cell lysates from mutant LRRK2 MEFs compared to WT cells. Inhibition of LRRK2 kinase partially restored cellular BMP levels, whereas inhibition of GCase further increased the BMP content. In isolated EVs from LRRK2 mutant cells, LRRK2 inhibition decreased BMP content whereas GCase inhibition tended to increase it. Using metabolic labeling experiments, we demonstrated that the increase in cellular BMP content is not due to an increase in BMP synthesis, even though we observed an increase in BMP synthesizing enzyme, CLN5, in LRRK2 mutant MEFs and patient-derived fibroblasts. Finally, pharmacological modulators of EV release confirmed that BMP release is associated with EV secretion. Together, these results establish LRRK2 as a regulator of BMP levels in cells and its release through EVs, with GCase activity further modulating this process in LRRK2 mutant cells. Mechanistic insights from these studies have implications for the potential use of BMP-positive EVs as a biomarker for Parkinson's disease and associated treatments.

## INTRODUCTION

Variants in the gene encoding Leucine rich repeat kinase 2 (*LRRK2*) and β-glucocerebrosidase (GCase; *GBA1*) together constitute the largest contributors to familial and sporadic Parkinson's disease (PD)[1]. Although G2019S is the most prevalent PD-associated *LRRK2* mutation, R1441G is more penetrant and is associated with an earlier disease onset[2-4]. A shared mechanism of pathogenesis among all PD-causing LRRK2 mutations is increased LRRK2 kinase activity, which leads to phosphorylation of its cognate Rab GTPase substrates, including Rab8, Rab10 and Rab12, that are key regulators of intracellular vesicle trafficking[5]. A prevailing hypothesis of pathogenesis in LRRK2 PD cases is that LRRK2 phosphorylation of Rabs results in defective autophagy and endo-lysosomal homeostasis and defective ciliogenesis in the nigrostriatal circuit[5,6].

*GBA1* encodes a lysosomal hydrolase, glucocerebrosidase (GCase), essential for glycosphingolipid degradation. Homozygous loss-of-function mutations in *GBA1* cause Gaucher's disease, a lysosomal storage disorder characterized by cytotoxic accumulation of lipid substrates of GCase, glucosylceramide and glucosylsphingosine; heterozygous carriers have a 5-10 fold increased risk of PD [7,8]. The predominant hypothesis for the pathogenic mechanism of *GBA1* variants is related to aberrant aggregation and clearance of alpha-synuclein in a feed-forward cascade[9,10]; a hypothesis being tested clinically using GCase activators. Additionally, we and others previously showed that GCase enzymatic function is modulated by LRRK2 kinase activity[11,12]. Altogether, it is possible that dysregulation of the endo-lysosomal biology is associated with pathogenic variants of both *LRRK2* and *GBA1*[6,13].

Bis(monoacylglycerol)phosphate (BMP, also known as LBPA or Lysobisphosphatidic acid) is an atypical, negatively-charged glycerophospholipid important for maintaining endo-lysosomal homeostasis[14]. BMP resides primarily in endo-lysosomal intralumenal vesicles (ILVs) where it participates in multiple processes, including cholesterol egress, exosome biogenesis and lipid catabolism[14,15]. Of note, BMP acts together with Saposin-C as enzymatic cofactors of GCase[16,17]. Multiple BMP isomers are present in cells, based on differences in their fatty acyl chains and their positions relative to the sn-2 and sn-3 carbon atoms on each of its two glycerol backbones[14,15]; the sn-2:sn-2' isomer is the proposed active form[18,19]. Dioleoyl-BMP (di-18:1-BMP) is the predominant form in numerous cell lines analyzed[20-23] and didocosahexaenoyl-BMP (di-22:6-BMP) is one of the most abundant species in the brain[24,25]. Fatty acyl composition is thought to influence BMP biophysical properties and function[26].

We and others recently reported elevated levels of total di-18:1-BMP and total di-22:6-BMP species in the urine of carriers of PD-associated *LRRK2* and *GBA1* mutations[27-29]. Although we did not observe

a correlation between urinary BMP and PD progression[28], these studies underscore BMP's utility as a patient enrichment and target modulation biomarker in therapeutic trials[30]. Based on our previous findings, in the present study we focused on these two BMP species.

Given the specific intracellular localization of BMP (in ILVs; exosomes when released) and its proposed roles in exosome biogenesis[19], we hypothesized that its increased levels in PD biofluids may be a consequence of an increase in the secretion of BMP containing extracellular vesicle (EV). To gain mechanistic insight into the regulation and biological significance of BMP release, we monitored BMP release in EVs and performed kinetic analyses of BMP biosynthesis in mouse embryonic fibroblasts (MEFs) from wild-type (WT) or R1441G LRRK2 knock-in mice. In addition, we examined the regulation of BMP by a LRRK2 kinase inhibitor, MLi-2, and a GCase inhibitor, conduritol β-epoxide (CBE), to gain insights into the role of BMP in potential therapeutic vs. pathophysiological responses, respectively. Our data indicate that LRRK2 and GCase activities modulate its release in EVs.

## RESULTS

### Analysis of BMP-positive endo-lysosomes in R1441G LRRK2 mouse embryonic fibroblasts

We first performed immunofluorescence microscopy of BMP-positive endo-lysosomes in both WT and R1441G LRRK2 knock-in MEFs. The overall antibody-accessible BMP pool was significantly decreased in mutant LRRK2-expressing cells compared to WT (Figure 1A, B). In contrast, endo-lysosomal LAMP2 fluorescence was higher in mutant LRRK2 MEFs (Figure 1A, C). Previous studies found structural defects in endo-lysosomes of different cell types harboring pathogenic LRRK2 mutations[31-33]. Since BMP is specifically enriched in intra-luminal vesicles (ILVs) in the endo-lysosomes where it regulates important catabolic reactions, we examined multivesicular endosome (MVE) morphology of these cells. In agreement with previous findings[33], transmission electron microscopy revealed decreased MVE area in R1441G LRRK2 MEFs (average area= 0.11 $\mu m^2$) compared to WT MEFs (average area= 0.27 $\mu m^2$) (Figure 1D, E). In addition, the overall endo-lysosomal ILV number was diminished in the R1441G LRRK2 cell line (Figure 1F). These data suggest that the pathogenic LRRK2 mutation alters BMP-positive endo-lysosome morphology and ILV content.

### LRRK2 and GCase activities modulate extracellular vesicle release

Given the previously described roles of BMP in ILV/exosome biogenesis, we investigated whether the alterations observed in antibody-accessible BMP and MVE ILV number in LRRK2 mutant MEFs could be explained by changes in EV release. We isolated and characterized EVs from both WT and R1441G MEFs and also assessed the effects of LRRK2 and GCase pharmacological inhibitors, MLi-2 and CBE,

respectively on EV content and number. Inhibition of LRRK2 kinase and GCase enzymatic activities was confirmed, respectively, by monitoring phospho-Rab10 levels in whole cell lysates and performing a fluorescence-based GCase activity assay in cells (Figure 2A, B). Consistent with our immunofluorescence data, upregulation of LAMP2 was observed in R1441G LRRK2 whole cell lysates (WCL; Figure 2 A, C, D and E), as previously reported in LRRK2 G2019S knock-in mouse brain[34]. MLi-2 treatment for 48 hours partially reversed this phenotype (Figure 2 A, C, E), suggesting that aberrant LRRK2 kinase activity influences endo-lysosomal homeostasis.

We next analyzed the profiles of isolated EV fractions from both wild-type (WT) and R1441G LRRK2 mutant MEFs. Both LAMP2 and Flotillin-1 were assessed to explore alterations in release of EV subpopulations; LAMP2 is enriched in ILV-derived EVs while Flotillin-1 is also seen in plasma membrane-derived ectosomes that reflect outward budding of the plasma membrane[35]. Biochemical analysis revealed an elevation of LAMP2, but not Flotillin-1, in EVs derived from R1441G LRRK2 MEFs compared to those from WT MEFs (Figure 2C, F, G). Upon MLi-2 treatment, a modest but significant decrease in both EV-associated protein markers was observed in isolated EV fractions from mutant LRRK2 MEFs (Figure 2C, F, G). In contrast, inhibition of GCase activity in mutant LRRK2 cells led to an increase in LAMP2, but not Flotillin-1, in isolated EVs compared to those derived from WT MEFs (Figure 2C, F, G). Finally, analysis of WT cell-derived EVs revealed no major differences in EV marker levels between untreated (control) and MLi-2- or CBE-treated conditions (Supplemental Figure 1A-C).

To complement these data, we conducted nanoparticle tracking analysis (NTA). Isolated EV fractions from WT and R1441G LRRK2 cells exhibited comparable particle size distributions (Supplemental Figure 1D). Treatments with MLi-2 and CBE yielded measurable quantitative changes in EV concentrations that did not reach statistical significance (Supplemental Figure 1E), potentially reflecting the inherent variability of NTA due to its inability to distinguish EVs from non-vesicular particles[37,38]. For the R1441G MEF cells, MLi-2 decreased EV concentration while CBE increased EV particles per ml, in agreement with the effects observed in our biochemical analysis.

Altogether these results suggest that EV secretion is influenced by LRRK2 kinase and GCase hydrolase activities; while MLi-2 treatment decreases EV release, CBE increases it.

**Targeted BMP lipid analysis in intact cells and extracellular vesicles**

Ultra-performance liquid chromatography-tandem mass spectrometry (UPLC-MS/MS) was used to measure quantitatively the impact of LRRK2 and GCase activities on BMP isoform abundance in cells

and isolated EV fractions. Remarkably, an overall increase in total BMP isoforms was detected in mutant LRRK2 MEF cell lysates (Figure 3A-D), with di-22:6-BMP and di-18:1-BMP as the major species. It is important to note that mass spectrometry-based methods detect total BMP content while antibody staining (Figure 1A, B) only detects so-called "antibody-accessible" BMP[39]. The mass spectrometry-based increase in total BMP in LRRK2 mutant cells indicates that this pool is less antibody-accessible than that present in wild type cells. Alternately, the anti-BMP antibody may be less specific and detect other analytes.

In R1441G cells, LRRK2 inhibition for 48 hours with MLi-2 decreased total di-22:6-BMP and total di-18:1-BMP levels by ~20% (Figure 3A and B). Conversely, inhibition of GCase increased total BMP levels, reaching significance for di-22:6-BMP levels compared with untreated, R1441G LRRK2 cells (Figure 3C). No statistically significant differences in intracellular BMP levels were observed in WT LRRK2 MEFs upon LRRK2 or GCase inhibition (Supplemental Figure 1D, E), suggesting a dominant role of mutant LRRK2 activity in BMP regulation. These data suggest that there are LRRK2-independent clonal differences leading to differences in basal BMP content between WT and mutant MEF cells; however, such clonal variation does not impact the effect of MLi-2 or CBE treatment in R1441G cells.

Analysis of isolated EV fractions detected only the di-18:1-BMP isoform, with no evidence of di-22:6-BMP. Although a trend toward higher di-18:1-BMP levels was observed in EVs derived from WT cells compared to those from mutant LRRK2 cells, this difference was not statistically significant (Figure 3E). Treatment of LRRK2 R1441G MEFs with MLi-2 resulted in a significant partial decrease in EV-associated total BMP (Figure 3E), consistent with previous observations in non-human primates and PD mouse models that showed decreased extracellular urinary BMP upon LRRK2 kinase pharmacological inhibition[40-42]. In contrast, inhibition of GCase activity yielded an opposite, albeit not significant, trend (Figure 3E). These latter findings may be explained by the observation that GCase inhibition by CBE was less pronounced in LRRK2 R1441G cells compared to WT cells under identical concentration and treatment duration conditions (Figure 2B). Finally, no significant differences in EV-associated BMP abundance between untreated (control) and MLi-2- or CBE-treated WT LRRK2 MEFs were observed (Supplemental Figure 1F).

In addition to analyzing BMP, we also examined GCase lipid substrates in both cells and isolated EVs. Targeted quantification of sphingolipid species revealed elevated GCase substrate abundance in both CBE-treated WT and mutant LRRK2 cells, validating the treatment paradigm used in this study. Interestingly, CBE-mediated accumulation of GCase substrates was more evident in R1441G LRRK2

than in WT cells (Supplemental Figure 2A). This suggests that, despite a less pronounced direct effect on GCase activity (Figure 2B), the R1441G mutation might contribute to broader endo-lysosome dysfunction, which could alter the dynamics of substrate accumulation. On the other hand, analysis of isolated EV fractions revealed lower levels of glucosylceramide, galactosylceramide, and glucosylsphingosine in EVs from R1441G LRRK2 cells compared to those from WT MEFs, but no significant differences were detected between control or CBE-treated conditions independent of LRRK2 mutation status (except for glucosylsphingosine, which showed an increase in WT-EVs upon GCase inhibition; Supplemental Figure 2B).

Altogether, given that BMP is specifically enriched in ILVs (which become exosomes upon release), the data presented above support our biochemical analysis (Figure 2C, D, F) and suggest a role for LRRK2 and GCase in modulating BMP release in association with LAMP2-positive exosomes from MEF cells.

**BMP biosynthesis is not influenced by LRRK2 kinase and GCase activities**

To rule out the possibility that differences in cellular and EV-associated BMP levels following MLi-2 or CBE treatment of R1441G cells were caused by alterations in BMP metabolism rather than changes in membrane trafficking and EV release, we performed metabolic labeling experiments using heavy (H) isotope-labeled 22:6 and 18:1 fatty acids as BMP precursors.

Cells were pulsed for 25_min with heavy isotope BMP precursors and then washed and chased for different time points (Figure 4A). UPLC-MS/MS analysis allowed us to differentiate unlabeled versus semi-labeled (H,L'; only one heavy isotope-labeled fatty acid chain) or fully-labeled (H,H'; both fatty acid chains heavy isotope-labeled) BMP species (Figure 4A). Initial experiments were performed over 48h using mutant LRRK2 cells under control and LRRK2- or GCase-inhibition conditions; untreated WT cells were included for comparison. Strikingly, even at time 0 and throughout the length of the experiment, R1441G LRRK2 cells displayed substantially higher H,L'- and H,H'-22:6-BMP species than WT cells (left and middle plots in Figure 4 B). H,L', but not H,H' 18:1-BMP was detected, which appeared to increase to a greater extent in R1441G LRRK2 cells at least during the initial 8h of the experiment (right plot, Figure 4 B). Despite these differences between WT and mutant LRRK2 cells, neither inhibition of LRRK2 or GCase had a major impact in the kinetics of BMP synthesis or catabolism (Figure 4B). To better resolve initial BMP synthesis rates, we reduced the pulse labeling time and chase time to 60 min. In this set of experiments, only isotope-labeled 22:6-BMP species were detected (Figure 4C), possibly reflecting a preference for 22:6 BMP synthesis by MEFs. As before, even at time 0 and throughout the 60 min duration of the assay, 22:6-BMP levels were consistently higher in

R1441G LRRK2 cells compared with WT MEFs. Again, no overall rate differences were seen between untreated and MLi-2- or CBE-treated cells. These experiments support the hypothesis that rather than altering BMP metabolic rates, LRRK2 and GCase activities influence EV-mediated BMP release.

**Increased BMP synthase protein expression in mutant LRRK2 cells**

To further investigate the biological significance of BMP upregulation observed in mutant LRRK2 MEF cells (Figure 3A-D; Figure 4B, C), we examined the expression of CLN5, a key lysosomal enzyme in the BMP biosynthetic pathway[43,44]. Interestingly, biochemical analysis of total cell lysates revealed a significant fold-change increase in CLN5 protein levels in R1441G LRRK2 MEFs relative to WT cells (Figure 5A). Notably, 16 hour treatment with MLi-2 reduced CLN5 levels to a comparable fold-change extent (Figure 5B). To validate these findings in a human and disease-relevant context, we examined CLN5 protein expression in cultured fibroblasts derived from Parkinson's disease (PD) patients carrying the G2019S LRRK2 mutation. Consistent with our observations in MEF cells, CLN5 protein levels were reduced following 16 hr MLi-2 treatment in a concentration-dependent manner (Figure 5C). Notably, the maximal reduction was observed at the same 200nM MLi-2 concentration used in MEF cell experiments, a dose that also did not induce observable cytotoxic effects in human fibroblasts. Similar results were obtained in patient-derived fibroblasts harboring the R1441G LRRK2 mutation (Figure 5D). Altogether, these data suggest that LRRK2 kinase activity may regulate CLN5 protein expression. The upregulation of CLN5 may be due to an overall upregulation of lysosomal enzymes as LAMP2 levels were also increased (Figure 2A, C, E). Moreover, the observed baseline differences in BMP, as documented in the flux study above (Figure 4B and C), could result from CLN5 upregulation. The lack of significant changes in the BMP synthesis rate (Figure 4B and C) suggests either a limitation in substrate availability or that CLN5 is operating at maximal capacity.

**BMP release is EV-mediated**

Our data suggest that BMP is exocytosed in association with EVs and that LRRK2 and GCase activities modulate BMP secretion. To determine the magnitude of BMP release via EV secretion, we assessed the impact of pharmacological modulators of EV release. Treatment of WT MEFs with GW4869, a selective type 2-neutral sphingomyelinase inhibitor, decreased EV release as monitored by reduced levels of LAMP2 and Flotillin-1 in EV fractions (Figure 6A). Under these conditions, we observed a parallel decrease in exosomal BMP (Figure 6A, B). In contrast, enhancing EV release with bafilomycin A1 (B-A1), a pharmacological inhibitor of the endo-lysosomal proton pump V-ATPase that dramatically boosts EV exocytosis[35,45], resulted in the opposite trend (Figure 6A, C): EV markers and BMP levels increased. Biochemical analysis of EV release in R1441G LRRK2 cells showed similar behavior as in WT

MEFs upon treatment with these agents (Figure 6A and Supplemental Figure 3). GW4869 inhibition of EV release increased cellular BMP content (Figure 5D), while enhanced EV release upon B-A1 treatment diminished intracellular total di-22:6-BMP and di-18:1-BMP (Figure 5E). Altogether, these results strongly support the notion that BMP is released by EV-mediated MVE exocytosis.

**DISCUSSSION**

Here we have shown that: (a) hyperactive LRRK2 kinase upregulates mass spectrometry-determined BMP levels and the extracellular vesicles (EVs) that relase BMP in MEF cells. (b) LRRK2 and GCase pharmacological inhibitors, MLi-2 and CBE, modulate BMP abundance in cells and isolated exosomal fractions in opposite directions without interfering with the kinetics of BMP biosynthetic or catabolic rates. While PD-associated mutations in *LRRK2* increase kinase activity, *GBA1* pathogenic variants are associated with decreased GCase enzymatic function. Therefore, MLi-2 treatment represents a potential therapeutic rescue, whereas CBE phenocopies pathogenic conditions. (c) Although the hyperactive kinase mutation is associated with an increase in the rate of BMP synthesis, neither MLi-2 or CBE affected BMP synthesis in the MEFs. (d) The expression of CLN5, a BMP synthase[43], is upregulated in mouse and patient-derived fibroblasts with PD-associated LRRK2 mutations, consistent with the flux data indicating elevated overall BMP synthesis. (e) Finally, BMP release was modulated by pharmacological agents known to modulate EV secretion. Together, these data indicate that the previously reported increase in urinary BMP levels in LRRK2 mutation carriers indicate dysregulated exocytosis of BMP-containing EVs.

Pioneering studies by Gruenberg and colleagues underscore the importance of BMP in endo-lysosome homeostastic regulation and generation of endo-lysosomal ILVs[14,18,19] that become exosomes upon release. Subsequent studies revealed that cellular levels of this atypical phospholipid are invariably altered in many neurodegenerative disorders characterized by endo-lysosome dysfunction[24]. Recently, key lysosomal enzymes involved in distinct steps of the BMP biosynthetic pathway were identified, including CLN5 which plays a critical role in this process[43,44]. Our microscopy analysis revealed decreased antibody-accessible BMP levels in R1441G LRRK2 cells. In contrast, our targeted lipid pathway analysis measurements consistently showed higher total BMP levels in R1441G LRRK2 cells compared with WT cells. As we have reported previously[39], BMP antibody detects only a sub-pool of “accessible” BMP while mass spectrometry detects all pools. Alternately, the antibody may also detect non-BMP analytes. Given the essential roles of BMP in endo-lysosomal catabolism, our immunofluorescence data predict that LRRK2 mutant cells have defective degradative capacity, consistent with recent reports[31,46]. In addition, we found a concomitant upregulation of LAMP2 and

the BMP-synthesizing enzyme CLN5, suggesting that LRRK2 may participate in endo-lysosome biogenesis regulation. Indeed, in macrophages and microglia, LRRK2 regulates the levels of multiple lysosomal proteins by inhibiting TFEB and MiTF[46], transcription factors that activate lysosome-related gene expression by binding to coordinated lysosomal expression and regulation (CLEAR) elements[47]. Although the promoter region of CLN5 contains a potential TFEB binding site[47], formal evidence for TFEB-mediated transcription of CLN5 is still lacking. The increase in CLN5 and LAMP2 protein levels may also reflect lysosomal stress[47]. Interestingly, MLi2 restored CLN5 levels in both murine MEFs and human fibroblasts, further providing support that BMP is a pharmacodynamic biomarker of not just target modulation but also a potential disease-relevant lysosomal pathway modulation. Our findings of CLN5 upregulation in mutant LRRK2 MEFs, validated by similar results in patient-derived fibroblasts, further establish MEFs as a relevant cellular model system for studying LRRK2 kinase activity and its therapeutic targeting[48-51].

We and others reported that BMP is aberrantly high in urine derived from LRRK2 and GBA mutation-carriers[27-29]. These results have also been reproduced in animal models, in which urinary BMP levels decrease upon administration of MLi-2 and other LRRK2 kinase inhibitors[40-42]. The present study complements these previous observations by providing evidence of EV-mediated BMP release that can be regulated by LRRK2 and GCase enzymatic activity. Consistent with this model, recent studies have shown that aberrant LRRK2 and GCase activities influence EV secretion in cellular and animal models of PD, including human patients[52-54]. Moreover, our data showing reduced EV release in mutant LRRK2 MEFs treated with MLi-2 is consistent with previous observations that LRRK2 kinase inhibition leads to surfactant accumulation in type 2 pneumocytes in the lung, likely as a consequence of impaired lysosome-related organelle exocytosis[41].

BMP is enriched in urinary EVs[55]. However, other studies did not detect BMP enrichment in isolated EV fractions and concluded that BMP may be present in ILVs of endo-lysosomal subpopulations devoted to degradative activities rather than exocytic events[56,57], as previously proposed[58]. Using our UPLC-MS/MS methodology, extracellular BMP can be efficiently detected in the urine of healthy and mutant LRRK2/GCase carriers[27-29], and additionally, in EV fractions derived from both WT and R1441G LRRK2 MEFs (this study). How does LRRK2 influence release of BMP-positive EVs (BMP-EVs)? A subset of Rab proteins that are master regulators of intracellular membrane trafficking pathways are important LRRK2 substrates[5]. Some of these Rabs include Rab10, Rab12 and Rab35, and have been shown to play regulatory roles in endo-lysosomal exocytosis and EV release[59,60]. We thus speculate that phosphorylation of one or several of these Rabs may lead to enhanced BMP release. Indeed,

G2019S LRRK2-–mediated Rab35 phosphorylation has been proposed to promote EV-mediated α-synuclein release and propagation between cells[61,62]. It is likely that aberrant LRRK2 and GCase activities trigger endo-lysosomal exocytosis, and associated release of BMP-containing EVs, via a so-called clearance pathway activated due to accumulation of cytotoxic endo-lysosomal substrates[63,64]. The contribution of these phosphorylated Rabs to EV-mediated BMP release will be of interest for future work.

In summary, this work provides evidence that LRRK2 and GCase pathological activities upregulate EV-mediated BMP release without altering its metabolism in cells. The observed changes induced by MLi-2 highlight the potential of LRRK2 inhibition as a therapeutic strategy to restore endo-lysosomal homeostasis by reducing BMP production and aberrant EV release. What is the clinical significance of elevated urinary BMP levels in PD patients? Inhibition of LRRK2 improves endo-lysosomal function[42], consistent with increased LRRK2 and decreased GCase activities associated with pathogenic variants which worsen endo-lysosomal homeostasis[6,13]; this may eventually lead to endo-lysosomal exocytosis followed by EV-mediate BMP release. We speculate that BMP-EVs may harbor a distinct molecular repertoire that could perhaps inform more precisely disease progression or pathobiology. Future investigations will be needed to study the contribution of dysfunctional LRRK2 and GCase in exocytosis of specific BMP-positive endo-lysosomal subpopulations and to further characterize the role of BMP-EVs in the context of disease pathophysiology but also as a PD diagnostic tool.

**ACKNOWLEDGMENTS**

This research was funded by a grant to K.M and A.L from The Michael J. Fox Foundation for Parkinson's Research (MJFF-019043).

**AUTHOR CONTRIBUTIONS**

K.M.M. and A.L. conceived the project with input from F.H. All experiments were carried out by E.M-S. and A.L. except for mass spectrometric analysis of BMP (F.H), and CLN5 biochemical analysis in human fibroblasts (M.C.). R.FS., M.E., A.G and M.J.M provided patient-derived fibroblasts. C.E. captured and analyzed transmission electron microscopy images. K.M., A.L., S.R.P. and F.H. oversaw the project. K.M. and A.L. obtained research funding. A.L. wrote and edited the manuscript with critical revision from all co-authors.

**COMPETING INTERESTS**

Following authors declare no competing non-financial interests but the following competing financial interests: Kalpana M. Merchant, PhD, has consulted for AcureX, Caraway, Nitrase, Nura Bio, Retromer Therapeutics, Sinopia Biosciences, Vanqua, Vida Ventures and the Michael J. Fox Foundation for Parkinson's Research. She has received research funding from the Michael J. Fox Foundation for Parkinson's Research. Albert Lu, MD, PhD, and Suzanne R. Pfeffer, Ph.D. have received research funding from the Michael J. Fox Foundation for Parkinson's Research. Frank Hsieh, PhD and Ms. Marianna Arnold are employed by Nextcea, Inc., which holds patent rights to the di-22:6-BMP and 2,2'-di-22:6-BMP biomarkers for neurological diseases involving lysosomal dysfunction (US 8,313,949, Japan 5,702,363, and Europe EP2419742).

**REFERENCES**


1. Smith LJ, Lee CY, Menozzi E, Schapira AHV. Genetic variations in GBA1 and LRRK2 genes: Biochemical and clinical consequences in Parkinson disease. Front Neurol. 2022;13:971252. doi:10.3389/fneur.2022.971252
2. Yue Z, Lachenmayer ML. Genetic LRRK2 models of Parkinson's disease: Dissecting the pathogenic pathway and exploring clinical applications. Mov Disord. 2011;26(8):1386-1397. doi:10.1002/mds.23737
3. Pont-Sunyer C, Tolosa E, Caspell-Garcia C, et al. The prodromal phase of leucine-rich repeat kinase 2-associated Parkinson disease: Clinical and imaging Studies. Mov Disord. 2017;32(5):726-738. doi:10.1002/mds.26964
4. Fan Y, Nirujogi RS, Garrido A, et al. R1441G but not G2019S mutation enhances LRRK2 mediated Rab10 phosphorylation in human peripheral blood neutrophils. Acta Neuropathol. 2021;142(3):475-494. doi:10.1007/s00401-021-02325-z
5. Pfeffer SR. LRRK2 phosphorylation of Rab GTPases in Parkinson's disease. FEBS Lett. 2022;10.1002/1873-3468.14492. doi:10.1002/1873-3468.14492
6. Roosen DA, Cookson MR. LRRK2 at the interface of autophagosomes, endosomes and lysosomes. Mol Neurodegener. 2016;11(1):73. doi:10.1186/s13024-016-0140-1
7. Sidransky E, Lopez G. The link between the GBA gene and parkinsonism. Lancet Neurol. 2012;11(11):986-998. doi:10.1016/S1474-4422(12)70190-4
8. Duran R, Mencacci NE, Angeli AV, et al. The glucocerobrosidase E326K variant predisposes to Parkinson's disease, but does not cause Gaucher's disease. Mov Disord. 2013;28(2):232-236. doi:10.1002/mds.25248

9. Fredriksen K, Aivazidis S, Sharma K, et al. Pathological α-syn aggregation is mediated by glycosphingolipid chain length and the physiological state of α-syn in vivo. Proc Natl Acad Sci U S A. 2021;118(50):e2108489118. doi:10.1073/pnas.2108489118
10. Stojkovska I, Wani WY, Zunke F, et al. Rescue of α-synuclein aggregation in Parkinson's patient neurons by synergistic enhancement of ER proteostasis and protein trafficking. Neuron. 2022;110(3):436-451.e11. doi:10.1016/j.neuron.2021.10.032
11. Ysselstein D, Nguyen M, Young TJ, et al. LRRK2 kinase activity regulates lysosomal glucocerebrosidase in neurons derived from Parkinson's disease patients. Nat Commun. 2019;10(1):5570. doi:10.1038/s41467-019-13413-w
12. Kedariti M, Frattini E, Baden P, et al. LRRK2 kinase activity regulates GCase level and enzymatic activity differently depending on cell type in Parkinson's disease. NPJ Parkinsons Dis. 2022;8(1):92. doi:10.1038/s41531-022-00354-3
13. Do J, McKinney C, Sharma P, Sidransky E. Glucocerebrosidase and its relevance to Parkinson disease. Mol Neurodegener. 2019;14(1):36. doi:10.1186/s13024-019-0336-2
14. Gruenberg J. Life in the lumen: The multivesicular endosome. Traffic. 2020;21(1):76-93. doi:10.1111/tra.12715
15. Gallala, H. D., & Sandhoff, K. (2011). Biological function of the cellular lipid BMP-BMP as a key activator for cholesterol sorting and membrane digestion. Neurochemical research, 36(9), 1594–1600. https://doi.org/10.1007/s11064-010-0337-6
16. Alattia JR, Shaw JE, Yip CM, Privé GG. Molecular imaging of membrane interfaces reveals mode of beta-glucosidase activation by saposin C. Proc Natl Acad Sci U S A. 2007;104(44):17394-17399. doi:10.1073/pnas.0704998104
17. Abdul-Hammed M, Breiden B, Schwarzmann G, Sandhoff K. Lipids regulate the hydrolysis of membrane bound glucosylceramide by lysosomal β-glucocerebrosidase. J Lipid Res. 2017;58(3):563-577. doi:10.1194/jlr.M073510
18. Kobayashi T, Stang E, Fang KS, de Moerloose P, Parton RG, Gruenberg J. A lipid associated with the antiphospholipid syndrome regulates endosome structure and function. Nature. 1998;392(6672):193-197. doi:10.1038/32440
19. Matsuo H, Chevallier J, Mayran N, et al. Role of LBPA and Alix in multivesicular liposome formation and endosome organization. Science. 2004;303(5657):531-534. doi:10.1126/science.1092425
20. Mason, R. J., Stossel, T. P., & Vaughan, M. (1972). Lipids of alveolar macrophages, polymorphonuclear leukocytes, and their phagocytic vesicles. The Journal of clinical investigation, 51(9), 2399–2407. https://doi.org/10.1172/JCI107052

21. Huterer, S., & Wherrett, J. (1979). Metabolism of bis(monoacylglycero)phosphate in macrophages. Journal of lipid research, 20(8), 966–973.
22. Bouvier, J., Zemski Berry, K. A., Hullin-Matsuda, F., Makino, A., Michaud, S., Geloën, A., Murphy, R. C., Kobayashi, T., Lagarde, M., & Delton-Vandenbroucke, I. (2009). Selective decrease of bis(monoacylglycero)phosphate content in macrophages by high supplementation with docosahexaenoic acid. Journal of lipid research, 50(2), 243–255. https://doi.org/10.1194/jlr.M800300-JLR200
23. Grabner, G. F., Fawzy, N., Schreiber, R., Pusch, L. M., Bulfon, D., Koefeler, H., Eichmann, T. O., Lass, A., Schweiger, M., Marsche, G., Schoiswohl, G., Taschler, U., & Zimmermann, R. (2020). Metabolic regulation of the lysosomal cofactor bis(monoacylglycero)phosphate in mice. Journal of lipid research, 61(7), 995–1003. https://doi.org/10.1194/jlr.RA119000516
24. Akgoc Z, Sena-Esteves M, Martin DR, Han X, d'Azzo A, Seyfried TN. Bis(monoacylglycero)phosphate: a secondary storage lipid in the gangliosidoses. J Lipid Res. 2015;56(5):1006-1013. doi:10.1194/jlr.M057851
25. Boland S, Swarup S, Ambaw YA, et al. Deficiency of the frontotemporal dementia gene GRN results in gangliosidosis. Nat Commun. 2022;13(1):5924. doi:10.1038/s41467-022-33500-9
26. Goursot A, Mineva T, Bissig C, Gruenberg J, Salahub DR. Structure, dynamics, and energetics of lysobisphosphatidic acid (LBPA) isomers. J Phys Chem B. 2010;114(47):15712-15720. doi:10.1021/jp108361d
27. Alcalay RN, Hsieh F, Tengstrand E, et al. Higher Urine bis(Monoacylglycerol)Phosphate Levels in LRRK2 G2019S Mutation Carriers: Implications for Therapeutic Development. Mov Disord. 2020;35(1):134-141. doi:10.1002/mds.27818
28. Merchant KM, Simuni T, Fedler J, et al. LRRK2 and GBA1 variant carriers have higher urinary bis(monacylglycerol) phosphate concentrations in PPMI cohorts. NPJ Parkinsons Dis. 2023;9(1):30. doi:10.1038/s41531-023-00468-2
29. Gomes S, Garrido A, Tonelli F, et al. Elevated urine BMP phospholipids in LRRK2 and VPS35 mutation carriers with and without Parkinson's disease. NPJ Parkinsons Dis. 2023;9(1):52. doi:10.1038/s41531-023-00482-4
30. Jennings D, Huntwork-Rodriguez S, Vissers MFJM, et al. LRRK2 Inhibition by BIIB122 in Healthy Participants and Patients with Parkinson's Disease. Mov Disord. 2023;38(3):386-398. doi:10.1002/mds.29297
31. Henry AG, Aghamohammadzadeh S, Samaroo H, et al. Pathogenic LRRK2 mutations, through increased kinase activity, produce enlarged lysosomes with reduced degradative capacity

and increase ATP13A2 expression. Hum Mol Genet. 2015;24(21):6013-6028. doi:10.1093/hmg/ddv314

32. Hockey LN, Kilpatrick BS, Eden ER, et al. Dysregulation of lysosomal morphology by pathogenic LRRK2 is corrected by TPC2 inhibition. J Cell Sci. 2015;128(2):232-238. doi:10.1242/jcs.164152
33. de Rus Jacquet A, Tancredi JL, Lemire AL, DeSantis MC, Li WP, O'Shea EK. The LRRK2 G2019S mutation alters astrocyte-to-neuron communication via extracellular vesicles and induces neuron atrophy in a human iPSC-derived model of Parkinson's disease. Elife. 2021;10:e73062. doi:10.7554/eLife.73062
34. Albanese F, Mercatelli D, Finetti L, et al. Constitutive silencing of LRRK2 kinase activity leads to early glucocerebrosidase deregulation and late impairment of autophagy in vivo. Neurobiol Dis. 2021;159:105487. doi:10.1016/j.nbd.2021.105487
35. Kowal J, Arras G, Colombo M, et al. Proteomic comparison defines novel markers to characterize heterogeneous populations of extracellular vesicle subtypes. Proc Natl Acad Sci U S A. 2016;113(8):E968-E977. doi:10.1073/pnas.1521230113
36. Mathieu M, Névo N, Jouve M, et al. Specificities of exosome versus small ectosome secretion revealed by live intracellular tracking of CD63 and CD9. Nat Commun. 2021;12(1):4389. doi:10.1038/s41467-021-24384-2
37. Gardiner C, Ferreira YJ, Dragovic RA, Redman CW, Sargent IL. Extracellular vesicle sizing and enumeration by nanoparticle tracking analysis. *J Extracell Vesicles*. 2013;2:10.3402/jev.v2i0.19671. doi:10.3402/jev.v2i0.19671
38. Bachurski D, Schuldner M, Nguyen PH, et al. Extracellular vesicle measurements with nanoparticle tracking analysis - An accuracy and repeatability comparison between NanoSight NS300 and ZetaView. *J Extracell Vesicles*. 2019;8(1):1596016. doi:10.1080/20013078.2019.1596016
39. Lu A, Hsieh F, Sharma BR, Vaughn SR, Enrich C, Pfeffer SR. CRISPR screens for lipid regulators reveal a role for ER-bound SNX13 in lysosomal cholesterol export. J Cell Biol. 2022;221(2):e202105060. doi:10.1083/jcb.202105060
40. Fuji RN, Flagella M, Baca M, et al. Effect of selective LRRK2 kinase inhibition on nonhuman primate lung. Sci Transl Med. 2015;7(273):273ra15. doi:10.1126/scitranslmed.aaa3634
41. Baptista MAS, Merchant K, Barrett T, et al. LRRK2 inhibitors induce reversible changes in nonhuman primate lungs without measurable pulmonary deficits. Sci Transl Med. 2020;12(540):eaav0820. doi:10.1126/scitranslmed.aav0820

42. Jennings D, Huntwork-Rodriguez S, Henry AG, et al. Preclinical and clinical evaluation of the LRRK2 inhibitor DNL201 for Parkinson's disease. Sci Transl Med. 2022;14(648):eabj2658. doi:10.1126/scitranslmed.abj2658
43. Medoh UN, Hims A, Chen JY, et al. The Batten disease gene product CLN5 is the lysosomal bis(monoacylglycero)phosphate synthase. Science. 2023;381(6663):1182-1189. doi:10.1126/science.adg9288
44. Singh S, Dransfeld UE, Ambaw YA, Lopez-Scarim J, Farese RV Jr, Walther TC. PLD3 and PLD4 synthesize S,S-BMP, a key phospholipid enabling lipid degradation in lysosomes. Cell. 2024;187(24):6820-6834.e24. doi:10.1016/j.cell.2024.09.036
45. Lu A, Wawro P, Morgens DW, Portela F, Bassik MC, Pfeffer SR. Genome-wide interrogation of extracellular vesicle biology using barcoded miRNAs. Elife. 2018;7:e41460. doi:10.7554/eLife.41460
46. Yadavalli N, Ferguson SM. LRRK2 suppresses lysosome degradative activity in macrophages and microglia through MiT-TFE transcription factor inhibition. Proc Natl Acad Sci U S A. 2023;120(31):e2303789120. doi:10.1073/pnas.2303789120
47. Sardiello M, Palmieri M, di Ronza A, et al. A gene network regulating lysosomal biogenesis and function. Science. 2009;325(5939):473-477. doi:10.1126/science.1174447
48. Dhekne HS, Yanatori I, Gomez RC, et al. A pathway for Parkinson's Disease LRRK2 kinase to block primary cilia and Sonic hedgehog signaling in the brain. *Elife*. 2018;7:e40202. doi:10.7554/eLife.40202
49. Sobu Y, Wawro PS, Dhekne HS, Yeshaw WM, Pfeffer SR. Pathogenic LRRK2 regulates ciliation probability upstream of tau tubulin kinase 2 via Rab10 and RILPL1 proteins. *Proc Natl Acad Sci U S A*. 2021;118(10):e2005894118. doi:10.1073/pnas.2005894118
50. Dhekne HS, Yanatori I, Vides EG, et al. LRRK2-phosphorylated Rab10 sequesters Myosin Va with RILPL2 during ciliogenesis blockade. *Life Sci Alliance*. 2021;4(5):e202101050. doi:10.26508/lsa.202101050
51. Kania E, Long JS, McEwan DG, et al. LRRK2 phosphorylation status and kinase activity regulate (macro)autophagy in a Rab8a/Rab10-dependent manner. *Cell Death Dis*. 2023;14(7):436. doi:10.1038/s41419-023-05964-0
52. Papadopoulos VE, Nikolopoulou G, Antoniadou I, et al. Modulation of β-glucocerebrosidase increases α-synuclein secretion and exosome release in mouse models of Parkinson's disease. Hum Mol Genet. 2018;27(10):1696-1710. doi:10.1093/hmg/ddy075

53. Cerri S, Ghezzi C, Ongari G, et al. GBA Mutations Influence the Release and Pathological Effects of Small Extracellular Vesicles from Fibroblasts of Patients with Parkinson's Disease. Int J Mol Sci. 2021;22(4):2215. doi:10.3390/ijms22042215
54. Maloney et al. LRRK2 Kinase Activity Regulates Parkinson's Disease-Relevant Lipids at the Lysosome. doi.org/10.1101/2022.12.19.521070
55. Rabia M, Leuzy V, Soulage C, et al. Bis(monoacylglycero)phosphate, a new lipid signature of endosome-derived extracellular vesicles. Biochimie. 2020;178:26-38. doi:10.1016/j.biochi.2020.07.005
56. Wubbolts R, Leckie RS, Veenhuizen PT, et al. Proteomic and biochemical analyses of human B cell-derived exosomes. Potential implications for their function and multivesicular body formation. J Biol Chem. 2003;278(13):10963-10972. doi:10.1074/jbc.M207550200
57. Laulagnier K, Motta C, Hamdi S, et al. Mast cell- and dendritic cell-derived exosomes display a specific lipid composition and an unusual membrane organization. Biochem J. 2004;380(Pt 1):161-171. doi:10.1042/BJ20031594
58. White IJ, Bailey LM, Aghakhani MR, Moss SE, Futter CE. EGF stimulates annexin 1-dependent inward vesiculation in a multivesicular endosome subpopulation. EMBO J. 2006;25(1):1-12. doi:10.1038/sj.emboj.7600759
59. Hsu C, Morohashi Y, Yoshimura S, et al. Regulation of exosome secretion by Rab35 and its GTPase-activating proteins TBC1D10A-C. J Cell Biol. 2010;189(2):223-232. doi:10.1083/jcb.200911018
60. Vieira OV. Rab3a and Rab10 are regulators of lysosome exocytosis and plasma membrane repair. Small GTPases. 2018;9(4):349-351. doi:10.1080/21541248.2016.1235004
61. Bae EJ, Kim DK, Kim C, et al. LRRK2 kinase regulates α-synuclein propagation via RAB35 phosphorylation. Nat Commun. 2018;9(1):3465. doi:10.1038/s41467-018-05958-z
62. Bae EJ, Lee SJ. The LRRK2-RAB axis in regulation of vesicle trafficking and α-synuclein propagation. Biochim Biophys Acta Mol Basis Dis. 2020;1866(3):165632. doi:10.1016/j.bbadis.2019.165632
63. Settembre C, Fraldi A, Medina DL, Ballabio A. Signals from the lysosome: a control centre for cellular clearance and energy metabolism. Nat Rev Mol Cell Biol. 2013;14(5):283-296. doi:10.1038/nrm3565
64. Tsunemi T, Perez-Rosello T, Ishiguro Y, et al. Increased Lysosomal Exocytosis Induced by Lysosomal Ca2+ Channel Agonists Protects Human Dopaminergic Neurons from α-Synuclein Toxicity. J Neurosci. 2019;39(29):5760-5772. doi:10.1523/JNEUROSCI.3085-18.2019

65. Carpenter AE, Jones TR, Lamprecht MR, et al. CellProfiler: image analysis software for identifying and quantifying cell phenotypes. Genome Biol. 2006;7(10):R100. doi:10.1186/gb-2006-7-10-r100
66. Liu N, Tengstrand EA, Chourb L, Hsieh FY. Di-22:6-bis(monoacylglycerol)phosphate: A clinical biomarker of drug-induced phospholipidosis for drug development and safety assessment. Toxicol Appl Pharmacol. 2014;279(3):467-476. doi:10.1016/j.taap.2014.06.014

**FIGURE LEGENDS:**

Figure 1. **Alterations of antibody-accessible BMP and endo-lysosomal morphology in LRRK2 R1441G-MEF cells. (A)** Confocal microscopy of endogenous BMP (green) and LAMP2 (red) immunofluorescence in WT and R1441G LRRK2 mutant MEF cells. Scale bar: 20µm. **(B-C)** Quantification of vesicular BMP intensity (**B**) and LAMP2 relative intensity (**C**) per cell area. Colored dots represent mean value from 4 independent experiments and violin plots show the distribution of individual cell data. Significance determined by two-tailed paired *t* test **p<0.01, ***p<0.001. **(D)** Representative transmission electron microscopy (TEM) images of Multivesicular endosomes (MVE) from WT and R1441G LRRK2 mutant MEF cells. MVB periphery highlighted in yellow. Scale bar: 250nm. **(E)** MVE area ($\mu m^2$) quantification in WT and R1441G LRRK2 mutant cells. Colored dots represent mean values from 3 independent experiments and violin plots show the distribution of individual cell data (35-45 cells/group). **(F)** Quantification of Intraluminal Vesicles (ILVs) per MVE in WT and R1441G mutant MEF cells. The number of ILVs per MVE are binned in three groups and plotted as a percentage of MVE from the total population of each experiment independently. Data from 3 independent experiments (mean ± SEM). Significance determined by two-tailed unpaired *t* test **(E)** and ordinary two-way ANOVA, uncorrected Fisher's LSD **(F)** *p<0.05, ****p<0.0001.

Figure 2. **LRRK2 and GCase activities modulate extracellular vesicle production. (A)** Whole cell lysates from WT and R1441G mutant MEF cells treated with 200nM MLi-2 for 24h were analyzed by western blotting. Representative images of LAMP2, phospho-Rab10 and α-Tubulin levels are shown. Molecular weight marker mobility is shown in kDa. **(B)** Flow cytometry measurement of GCase activity using PFB-FDGlu fluorescent GCase substrate in WT and R1441G LRRK2 mutant MEF cells treated with 300µM CBE for 24h. **(C-D)** Whole cell lysates (WCL) and isolated extracellular vesicles (EVs) from WT and R1441G LRRK2 mutant MEF cells treated with 200nM MLi-2 **(C)** or 300µM CBE **(D)** for 48h were analyzed by western blotting. Representative images of LAMP2, Flotillin-1 and α-Tubulin levels are shown. Molecular weight marker mobility is shown in kDa. **(E-G)** Quantification of LAMP2 and

Flotillin-1 levels relative to R1441G LRRK2 MEF cells in whole cell lysates (WCL). **(E)** and isolated EVs **(F-G).** Data from 6-9 independent experiments (mean ± SEM). Significance determined by two-tailed paired *t* test compared to R1441G LRRK2 control *p<0.05, **p<0.01, ****p<0.0001.

Figure 3. **Targeted lipid pathway analysis of BMP abundance in cellular and isolated EV fractions. (A-D)** UPLC-MS/MS determination of BMP isoforms normalized to protein content from cells treated with 200nM MLi-2 **(A-B)** or 300µM CBE **(C-D)** for 48h. Data shown as fold change relative to R1441G LRRK2 control MEF cells. Only BMP isoforms that were detected are shown. **(E)** UPLC-MS/MS determination of BMP isoforms normalized to protein content in EVs isolated from cells treated with 200nM MLi-2 or 300µM CBE for 48h. Only BMP isoforms that were detected are shown. Data from 3-6 independent experiments (mean ± SEM). Significance determined by ordinary one-way ANOVA, uncorrected Fisher's LSD **(A-D)** and one-way ANOVA with the Geisser-Greenhouse correction, uncorrected Fisher's LSD **(E)** *p<0.05, **p<0.01, ***p<0.001, ****p<0.0001.

Figure 4. **Inhibition of LRRK2 or GCase activities does not significantly impact BMP biosynthetic and catabolic rates. (A)** Schematic representation of the BMP metabolic labeling protocol with deuterated docosahexaenoic acid and $^{13}$C-labeled oleic acid. WT and R1441G mutant MEF cells were incubated with a pulse of DHA-d5 / OA-$^{13}$C for 20min, followed by a chase for different times. Cells were then collected for subsequent BMP lipidomic analysis. Structures of unlabeled (L) and isotope-labeled (H) fatty acids are shown in black or red, respectively. **(B-D)** UPLC-MS/MS determination of BMP isoforms normalized to protein content from WT MEF cells and R1441G LRRK2 mutant MEF cells ± MLi-2 (200nM) or CBE (300µM). Long **(B-C)** and short **(D)** chase time points shown as fold change relative to WT control MEF cells time 0. Only BMP isoforms that were detected are shown. Data from 3 replicated experiments (mean ± SEM).

Figure 5. **LRRK2 activity modulates CLN5 expression levels. A)** Whole cell lysates from WT and R1441G LRRK2 MEF cells were analyzed by western blotting. Representative immunoblots of CLN5, phospho-Rab10 (pRab10) and α-Tubulin are shown from two (#1 and #2) out of six independent experiments. Molecular weight marker mobility is shown in kDa. Plot at the bottom shows quantification of CLN5 immunoblot levels relative to WT and R1441G LRRK2 MEF cells**. B)** Whole cell lysates from R1441G LRRK2 MEF cells treated with 200nM MLi-2 for 24h were analyzed by western blotting. Representative immunoblots of phosphor-LRRK2 (pLRRRK2), CLN5 and α-Tubulin levels are shown from two (#1 and #2) out of three independent experiments. Molecular weight marker mobility is shown in kDa. Plot at the bottom shows quantification of CLN5 immunoblot levels in whole cell lysates of R1441G LRRK2 MEF cells untreated or MLi-2-treated**. C)** Whole cell lysates from G2019S LRRK2

patient-derived fibroblasts treated with indicated increasing MLi-2 concentrations for 24h were analyzed by western blotting. Immunoblots of CLN5, phospho-Rab10 (pRab10) and α-Tubulin levels are shown from one representative experiment (n=6 per condition, obtained from two independent replicate experiments using fibroblast cell lines derived from three different patients). Molecular weight marker mobility is shown in kDa. Plot at the bottom shows quantification of CLN5 immunoblot levels relative to G2019S LRRK2 patient-derived fibroblasts treated with MLi-2 at the indicated concentrations**. D)** Whole cell lysates from R1441G LRRK2 patient-derived fibroblasts treated with indicated increasing MLi-2 concentrations for 24h were analyzed by western blotting. Immunoblots of CLN5, phospho-Rab10 (pRab10) and α-Tubulin levels are shown from one representative experiment. In **A)** and **B)** significance determined by two-tailed, unpaired *t* test; significance in (**C**) determined by Dunnett's One-way ANOVA test; *p<0.05, ***p<0.001.

Figure 6. **Pharmacological modulation of EV-mediated BMP exocytosis. (A)** Whole cell lysates (WCL) and isolated EVs from WT MEF cells treated with 10µM GW4869 or 10nM bafilomycin-A1 (B-A1) for 24h were analyzed by western blotting. Representative immunoblots of LAMP2, Flotillin-1 and α-Tubulin are shown. Molecular weight marker mobility is shown in kDa. **(B-C)** UPLC-MS/MS determination of BMP isoforms normalized to protein content from WT MEF cells treated with 10nM B-A1 **(B)** or 10µM GW4869 **(C)** for 24h. Data shown as fold change relative to WT control MEF cells. Only BMP isoforms that were detected are shown. Data from 6 independent experiments (mean ± SEM). Significance determined by two-tailed unpaired *t* test *p<0.05, **p<0.01, ***p<0.001, ****p<0.0001. **(D-E)** Quantitation of BMP isoforms normalized to protein content in EVs isolated from MEF WT cells treated with 10nM B-A1 **(D)** or 10µM GW4869 **(E)** for 24h. Data shown as fold change relative to WT control MEF cells. Only BMP isoforms that were detected are shown. Data from 3 independent experiments (mean ± SEM). Significance determined by two-tailed unpaired *t* test *p<0.05, **p<0.01, ***p<0.001.

Supplemental Figure 1. **Further characterization of MEF-derived EV fractions. (A-C)** No significant differences in EV release between MLi-2/CBE–treated and untreated WT MEF cells. Quantification of LAMP2 and Flotillin-1 levels relative to WT control MEF cells in WCL **(A)** and isolated EVs **(B-C).** Data from 7-8 independent experiments (mean ± SEM). Significance determined by ordinary one-way ANOVA, uncorrected Fisher's LSD. **(D)** and **(E)**, Characterization of WT or R1441G LRRK2 MEF-derived purified EVs by Nanoparticle Tracking Analysis (NTA). **(D)** Representative plots of EV size distribution in each indicated condition. **(E)** Yield comparison of MEF-derived EVs from each indicated condition determined by NTA. Each colored dot represents an independent experiment. **(F-H)** No significant differences in EV-associated BMP levels between MLi-2/CBE–treated and untreated WT MEF cells. UPLC-MS/MS measurements of cellular **(F-G)** and EV-associated **(H)** BMP isoforms normalized to

protein content from cells treated with 200nM MLi-2 or 300µM CBE for 48h or left untreated (ctrl). Data shown as fold change relative to WT control MEF cells. Only BMP isoforms that were detected are shown. Data from 6-7 independent experiments (mean ± SEM). Significance determined by ordinary two-tailed paired *t* test; ns, not significant.

Supplemental Figure 2. **Quantitative analysis of GCase substrates in MEF cells and EV fractions. (A-B)** Lipidomic determination of Glucosylceramide (GlcCer), Galactosylceramide (GalCer) and Glucosylsphingosine (GlcSph) isoforms normalized to protein content from WT and R1441G LRRK2 mutant MEF cells **(A)** and isolated EVs **(B)** treated with 300µM CBE or 200nM MLi-2 for 48h. Heatmap showing values as fold change relative to R1441G LRRK2 mutant MEF cell control. Only GlcCer, GalCer and GlcSph isoforms that were detected are shown. Data from 3-9 independent experiments (mean ± SEM). Significance determined by ordinary two-way ANOVA, uncorrected Fisher's LSD *p<0.05, **p<0.01, ***p<0.001 ****p<0.0001.

Supplemental Figure 3. **Pharmacological modulation of EV-mediated BMP exocytosis in mutant LRRK2 MEF cells.** Whole cell lysates (WCL) and isolated EVs from R1441G LRRK2 MEF cells treated with 10µM GW4869 or 10nM bafilomycin-A1 for 24h were analyzed by western blotting. Representative images of LAMP2, Flotillin-1 and α-Tubulin levels are shown. Molecular weight marker mobility is shown in kDa.

**MATERIALS AND METHODS:**

**Cell culture, antibodies and other reagents–**Wild type (WT) and R1441G LRRK2 mutant MEF cells were grown in Dulbecco's modified Eagle's media (DMEM) containing 10% fetal bovine serum, 2 mM L-glutamine, and penicillin (100 U/ ml)/streptomycin (100 mg/ml). Cell lines were cultured at 37˚C with 5% CO2. Extracellular vesicle-free media was prepared by overnight ultracentrifugation of DMEM or RPMI supplemented with 10% FBS at 100,000 X g in a SW32Ti rotor. For bafilomycin-A1 (Sigma-Aldrich; catalog no. B1793) and GW4869 (SelleckChem; catalog no. S7609), the drug was added to cell media at 10 nM and 10 µM respectively and cells were cultured for 24 h before exosome collection. For MLi-2 (Tocris Bioscience; catalog no. 5756) and Conduritol B Epoxide (MERK; catalog no. 234599), the drug was added to cell media at 200nM and 300µM respectively and cells were cultured for 48 h before exosome isolation. 0.167mM Oleic acid (Cambridge Isotope Laboratories; catalog no. DLM-10012-0.001) and Docosahexaenoic acid (Cambridge Isotope Laboratories; catalog no. DLM-10012-0.001) were conjugated with 0.0278mM fatty acid–free BSA (Sigma-Aldrich; A8806) at a 1:6 molar ratio. Primary antibodies diluted in PBS with 1% BSA (for immunofluorescence) or 5% skim milk (for immunoblotting) were mouse anti–lysobisphosphatidic acid (anti-BMP) clone 6C4 1:1000 (EMD Millipore; catalog no. MABT837), rat monoclonal anti-mouse LAMP2 1:1000 (Developmental Studies Hybridoma Bank, catalog no.GL2A7), mouse anti-Flotillin-1 1:1000 (BD Biosciences; catalog no.610821), rabbit anti-

phospho-Rab10 1:1000 (Abcam; catalog no. ab230261), mouse anti-alpha tubulin 1:10000 (SigmaAldrich; catalog no. T5168), rabbit anti-CLN5 1:000 (Abcam; catalog no. ab170899), rabbit anti-phosphoLRRK2 1:000 (Abcam; catalog no. ab133450).

**Immunofluorescence–** Wild type (WT) and R1441G LRRK2 mutant MEF cells were fixed with 3.7% (v/v) paraformaldehyde for 15 min, washed and permeabilized/blocked with 0.1% saponin/1% BSA-PBS before staining with anti-LAMP2 and anti-BMP antibodies followed by goat anti-rat AlexaFluor555 and donkey anti-mouse AlexaFluor488. Nuclei were stained using 0.1 mg/ml DAPI (SigmaAldrich; catalog no. D9542). Coverslips were mounted on glass slides with Mowiol. Microscopy images were acquired using a Zeiss LSM880 laser scanning spectral confocal microscope (Carl Zeiss) equipped with an Axio Observer 7 inverted microscope, a blue diode (405 nm), argon (488 nm), diode-pumped solid-state (561 nm), and HeNe (633 nm) lasers, and a Plan Apochromat 63×/NA1.4 oil-immersion objective lens. DAPI, Alexa Fluor 488, Alexa Fluor 555 were acquired sequentially using 405-, 488- and 561-nm laser lines; Acousto-Optical Beam Splitter as a beam splitter; and emission detection ranges 415–480 nm, 500–550 nm, 571–625 nm, respectively. The confocal pinhole was set at 1 Airy unit. All images were acquired in a 1,024 × 1,024–pixel format. BMP and LAMP2 intensities were quantified using CellProfiler[65].

**Immunoblotting–**Cells were lysed in lysis buffer (50 mM Hepes, 150 mM KCl, 1% Triton X-100, 5 mM MgCl2, pH 7.4) supplemented with a protease/ phosphatase inhibitor cocktail (1mMNa3VO4, 10mMNaF, 1 mM PMSF, 10 µg/ml leupeptin, and 10 µg/ml aprotinin). After centrifugation at 12,000 g for 10 min, protein concentrations were measured in the cleared lysates. Equal amounts were resolved by SDS-PAGE followed by immunoblot analysis. Exosome final pellets were resuspended in SDS-PAGE loading dye (50 mM Tris-HCl pH 6.8, 6% glycerol, 2% SDS, 0.2% bromophenol blue), heated briefly at 95°C, resolved by 10% SDS-PAGE gel and transferred onto nitrocellulose membranes (Bio-Rad Laboratories; catalog no. 1620115) using a Bio-Rad Trans-Blot system. Membranes were blocked with 5% skim milk in TBS withTween-20 for 60 min at RT. Primary antibodies were diluted in blocking buffer and incubated overnight at 4°C. HRP-conjugated secondary antibodies (Bio-Rad Laboratories) diluted in blocking buffer at 1:3000 were incubated for 60 min at RT and developed using EZ-ECL (Biological Industries) or SuperSignal West Femto (Thermo Scientific; catalog no. 34094). Blots were imaged using an ImageQuant LAS 4000 system (GE Healthcare) and quantified using ImageJ software.

**Transmission Electron Microscopy–**Cells in culture were washed in PBS and fixed for 1h in 2.5% glutaraldehyde in 0.1 M phosphate buffer (PB) at RT. Next, samples were slowly and gently scraped and pelleted in 1.5 ml tubes. Pellets were washed in PB and incubated with 1% OsO4 for 90 min at 4 °C. Then samples were dehydrated, embedded in Spurr and sectioned using Leica ultramicrotome (Leica Microsystems). Ultrathin sections (50–70 nm) were stained with 2% uranyl acetate for 10 min, a lead-staining solution for 5 min and observed using a transmission electron microscope, JEOL JEM-1010 ftted with a Gatan Orius SC1000 (model 832) digital camera. Multivesicular Endosomes (MVE) and Intralumenal Vesicles (ILV) were identified by morphology and MVE area and ILV number were measured using ImageJ.

**Extracellular vesicle isolation–**MEF adherent cell cultures were seeded at 3-4*$10^6$ cells/plate in EV-free complete DMEM and grown for 24–48 h. Cell cultures were centrifuged at 300 g,

5 min to pellet cells, and supernatants were centrifuged again at 2100 g, 20 min to pellet dead cells. After this, filtration through 0.22 mm filter units was performed. Filtered media were ultracentrifuged for 75 min at 100,000 g in SW32Ti rotor to pellet extracellular vesicles. The supernatant was discarded, and the pellet (small EVs) re-suspended in phosphate-buffered saline (PBS) and centrifuged again for 75 min at 100,000 g in 140AT rotor. exosome pellets were frozen and stored at -80°C prior to further processing.

**Lipidomic analysis–**Targeted quantitative ultra-performance liquid chromatography tandem mass spectrometry was used to accurately quantitate the three geometrical isomers (2,2-, 2,3- and 3,3-) of di-22:6-BMP and di-18:1-BMP in control or treated MEF cells. Lipidomic analyses were conducted by Nextcea, Inc. as previously described[66]. Standard curves were prepared using authentic BMP reference standards. Protein was determined by bicinchoninic acid protein assay. A multiplexed quantitative ultraperformance liquid chromatography tandem mass spectrometry method was used to simultaneously quantitate sample glucosylceramides (GluCer d18:1/16:0, d18:1/18:0, d18:1/22:0, d18:1/24:0, d18:1/24:1), galactosylceramides (GalCer d18:1/16:0, d18:1/18:0, d18:1/22:0, d18:1/24:0, d18:1/24:1), glucosylsphingosine (GluSph 18:1), and galactosylsphingosine (GalSph 18:1). Standard curves were prepared from related standards using a class-based approach. Internal standards were used for each analyte reported. A SCIEX Triple Quad 7500 mass spectrometer was used in positive electrospray ionization mode for detection (SCIEX, Framingham, MA, USA). Injections were made using a Shimadzu Nexera XR UPLC (ultraperformance liquid chromatography) system (Shimadzu Scientific Instruments, Kyoto, Japan). The instruments were controlled by SCIEX OS 2.0 software.

**Metabolic labeling–**WT and R1441G LRRK2 mutant MEF cells were treated with 200nM MLi-2 or 300µM CBE for 16h. Cells were washed twice with PBS and incubated in serum-free DMEM ± MLi-2 or CBE for 1h. Next, Incubate cells in 0.167mM 13C-labeled Oleic Acid (OA) and 0.167mM deuterated docosahexaenoic acid (DHA) in serum-free DMEM containing 0.0278mM BSA for 25 min. Cells were washed with serum-free DMEM and chased with serum-free DMEM for short time points (0, 15, 30, 45, 60min) or complete DMEM for long timepoints (8, 24 and 48h). Cells were washed with PBS, trypsinized and collected in cold PBS. Cells were pelleted by centrifugation at 1000rpm for 7min and stored at -80°C prior to further processing.

**GCase activity–**GCase activity was measured by using the fluorogenic substrate PFB-FDGlu (Invitrogen, Carlsbad, CA). WT and R1441G LRRK2 mutant MEF cells were treated with 300µM CBE for 24h. After this, 150 µg/ml PFB-FDGlu (Thermo Fisher) was then added to cells followed by incubation for 2h at 37°C. Cells were then washed twice with PBS, trypsinized and fixed in cold 2% paraformaldehyde-PBS for 30 min. Cells were washed twice in PBS before assayed on a FACS analyzer (FACScan; BD) equipped with a 488 nm laser and 530 nm-FITC filter. Data were analyzed using Flowjo software (Tree Star).

**Statistics–**Results are expressed as the mean ± SEM. Means were compared using Student's t test when two experimental conditions were independently compared. Unless otherwise noted, statistical significance between multiple comparisons was assessed via one-way or two-way ANOVA with uncorrected Fisher's LSD test using GraphPad Prism version 9.

Figure 1 Meneses-Salas et al.

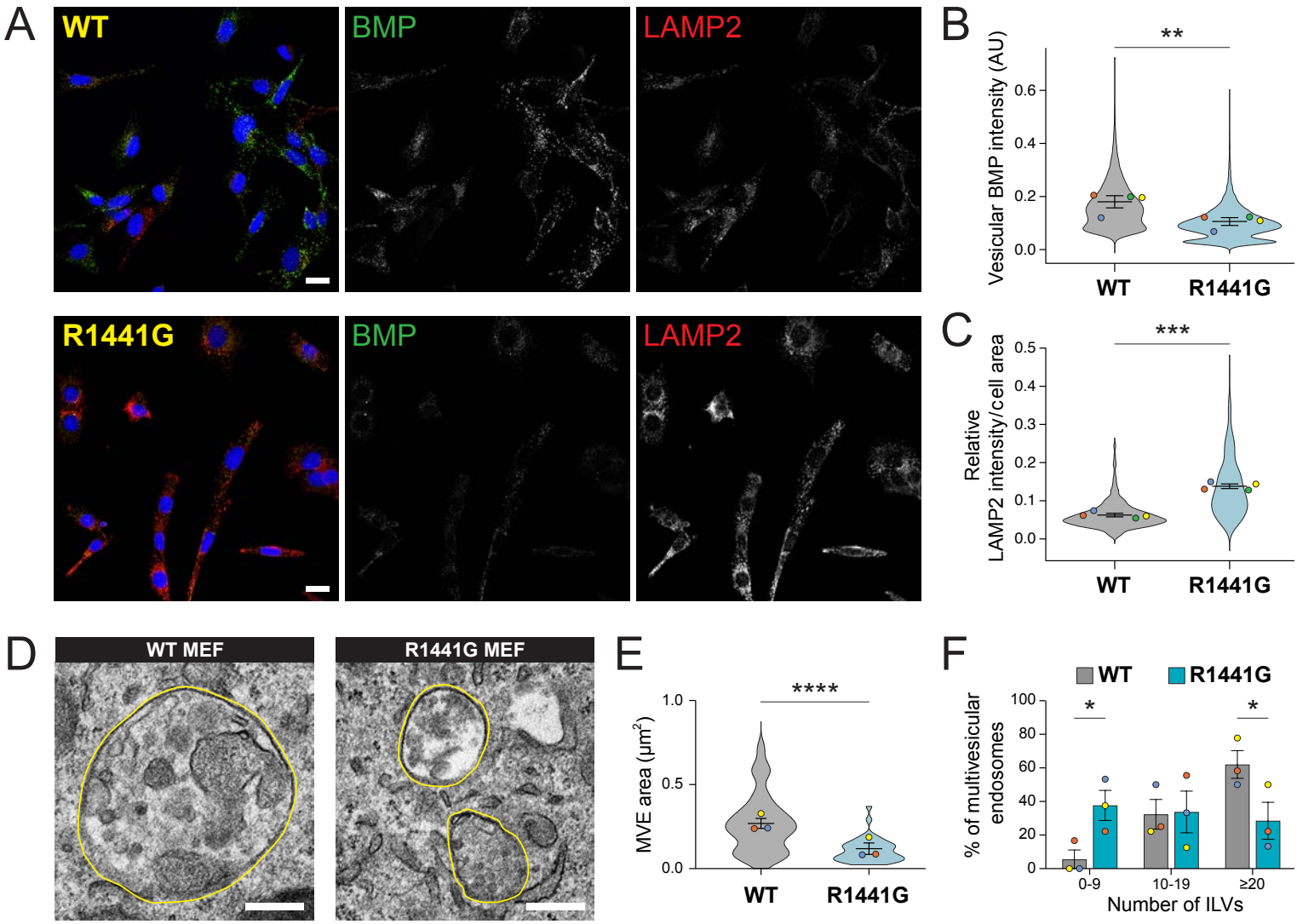

# Figure 2 Meneses-Salas et al.

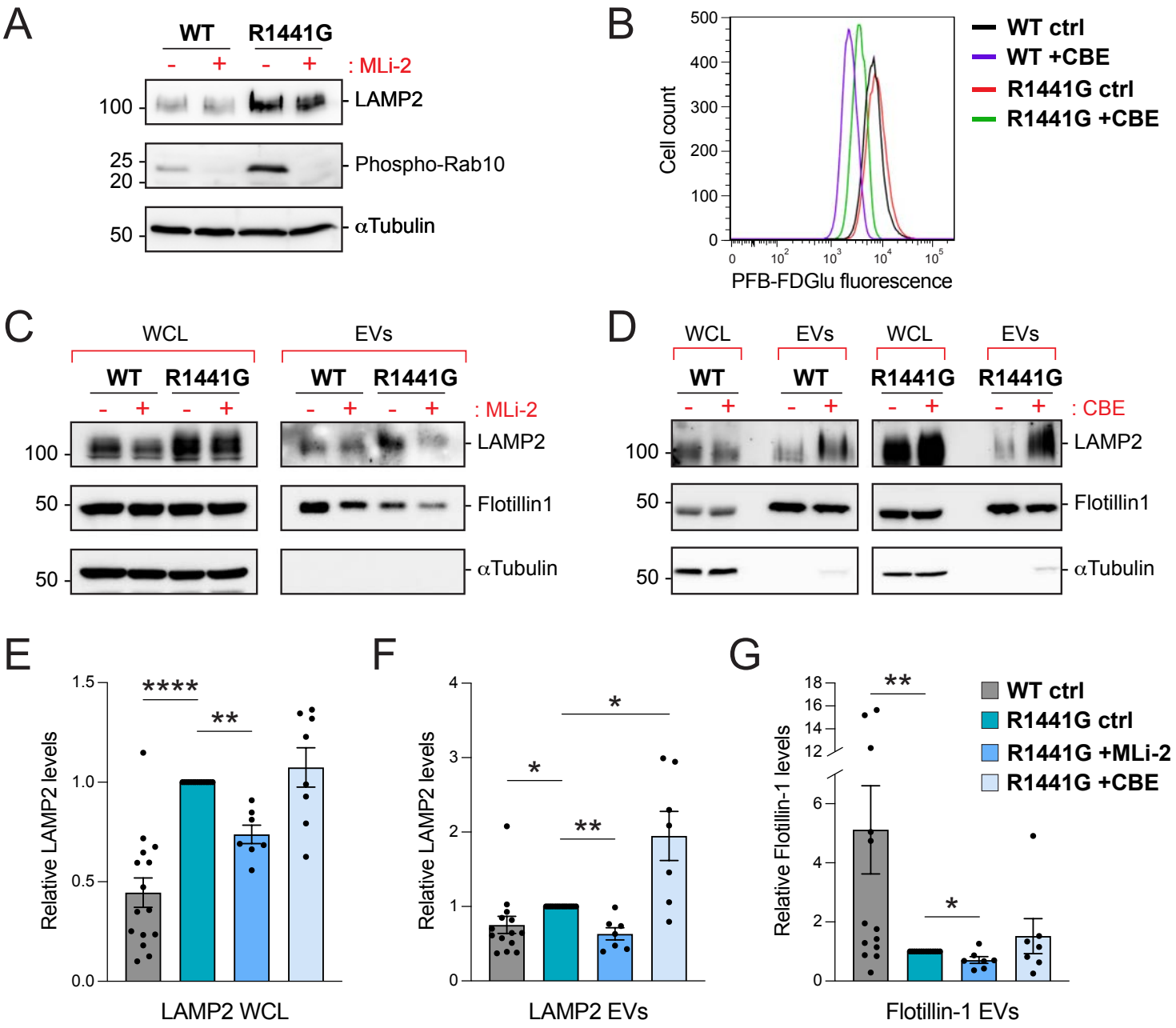

# Figure 3 Meneses-Salas et al.

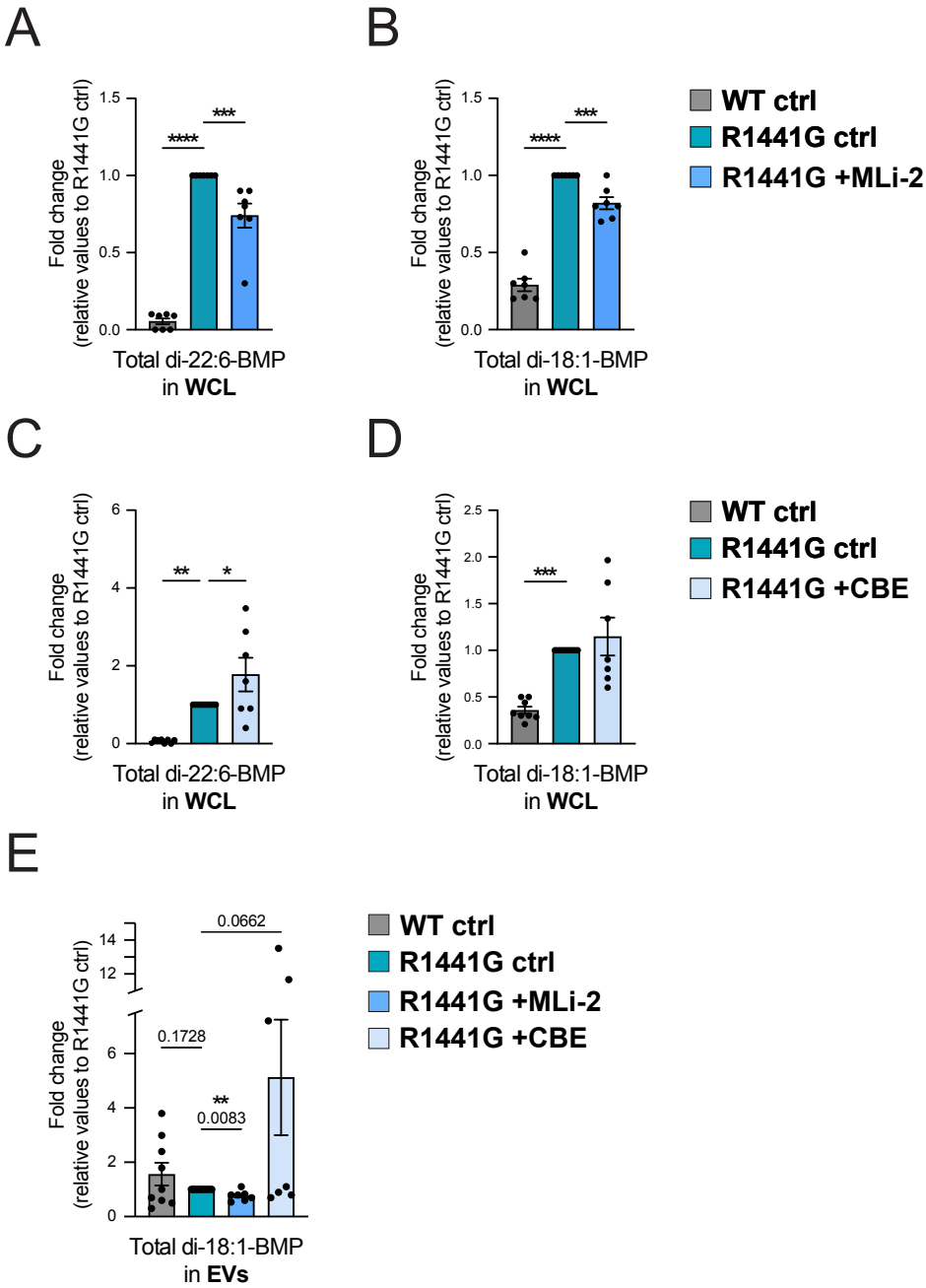

# Figure 4 Meneses-Salas et al.

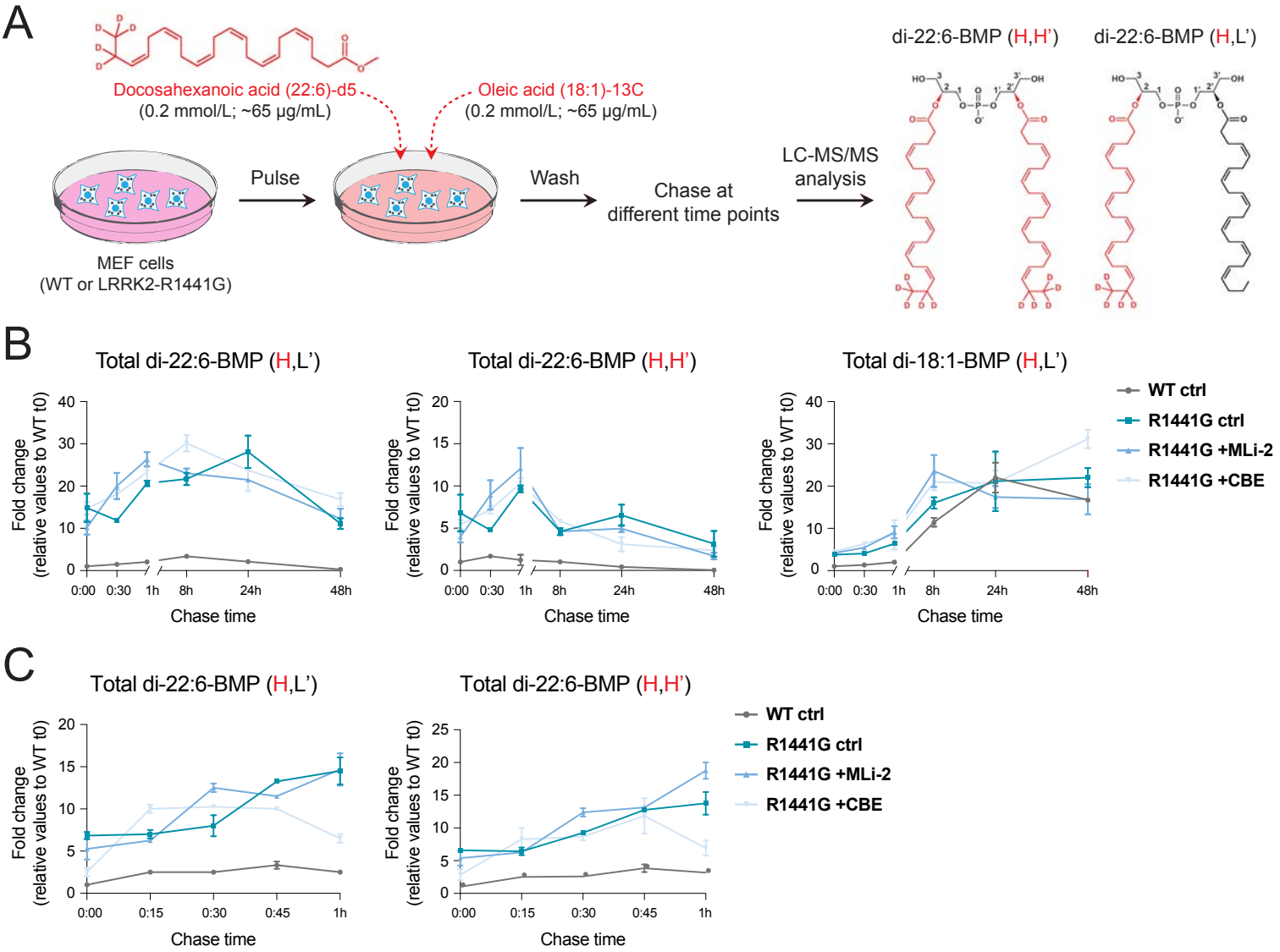

Figure 5 Meneses-Salas et al.

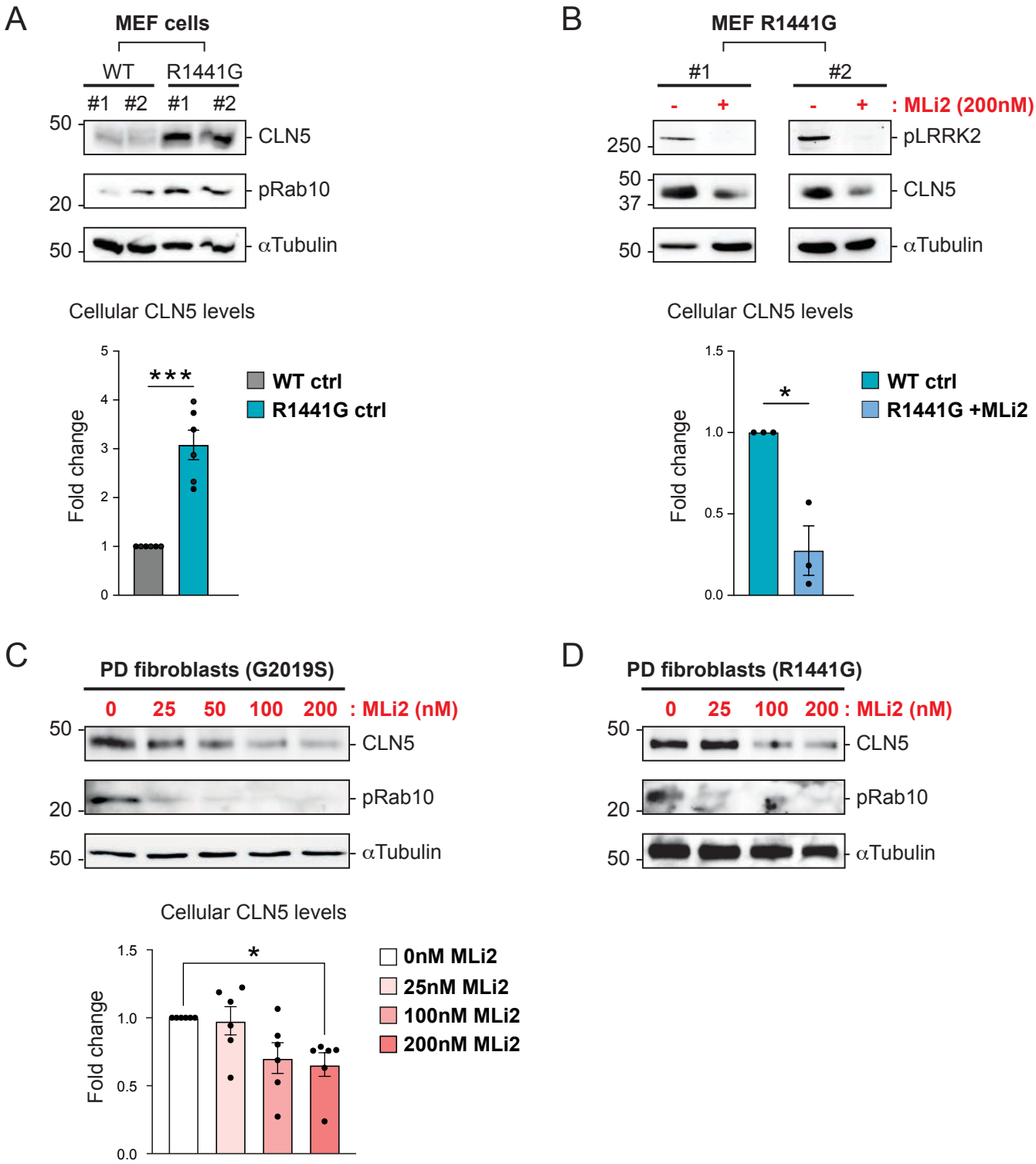

# Figure 6 Meneses-Salas et al.

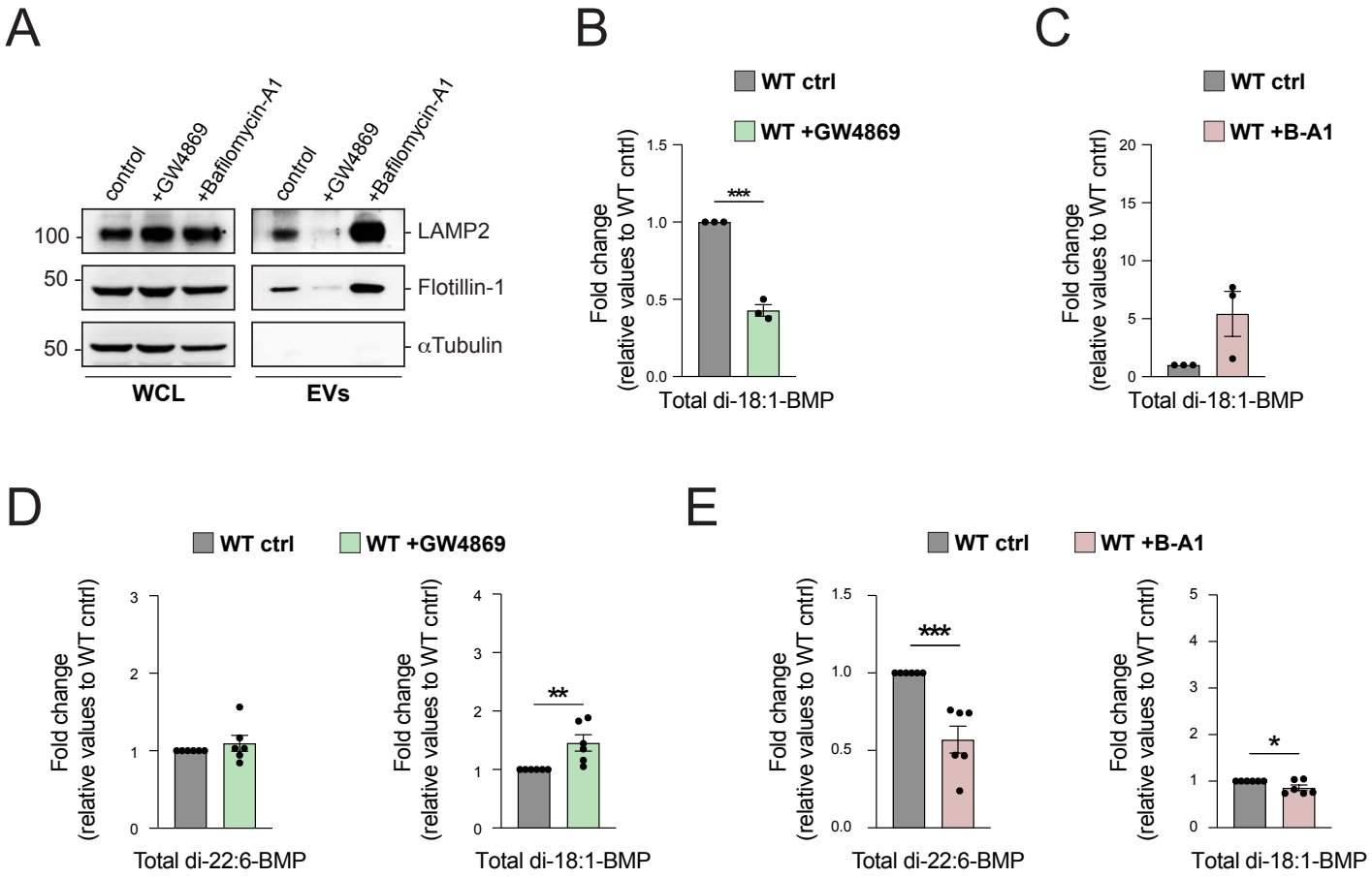

# Supplemental Figure 1 Meneses-Salas et al.

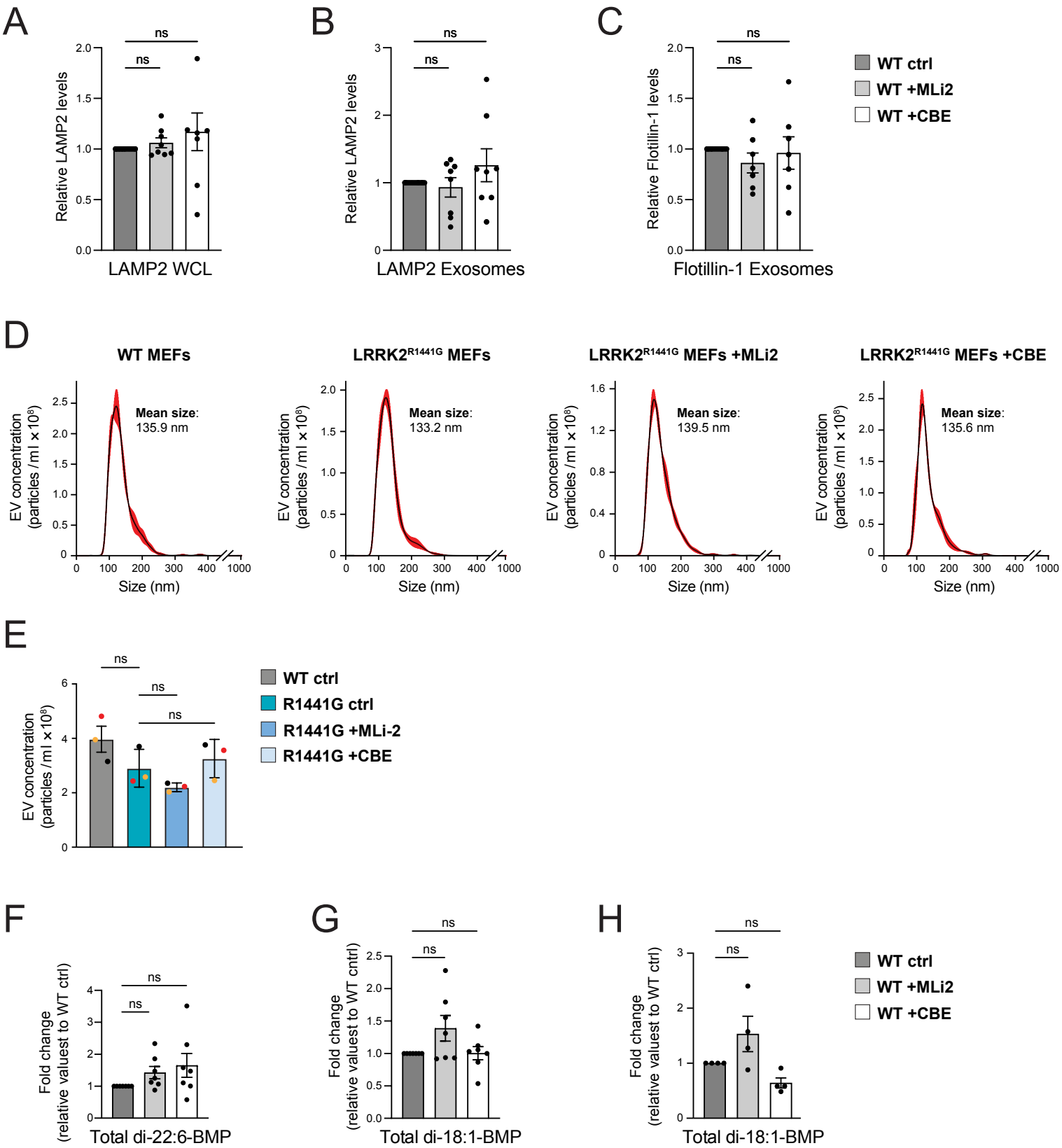

# Supplemental Figure 2 Meneses-Salas et al.

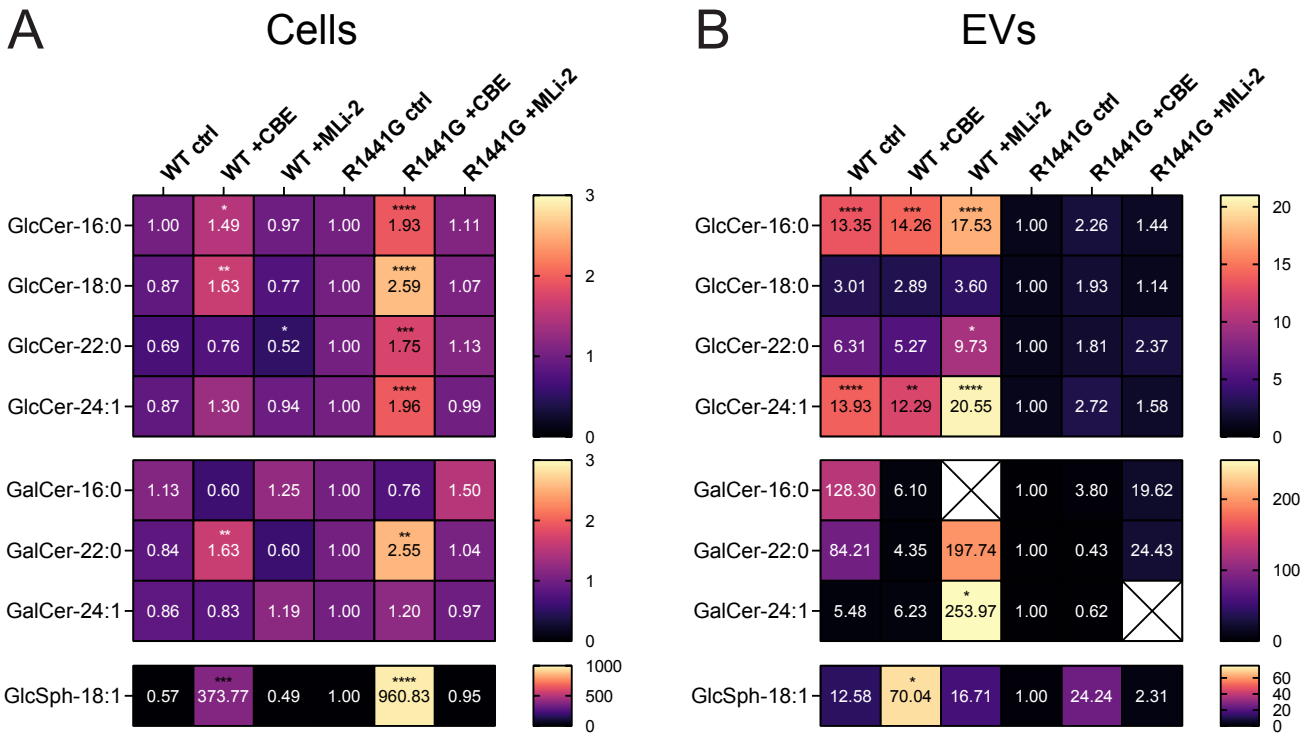
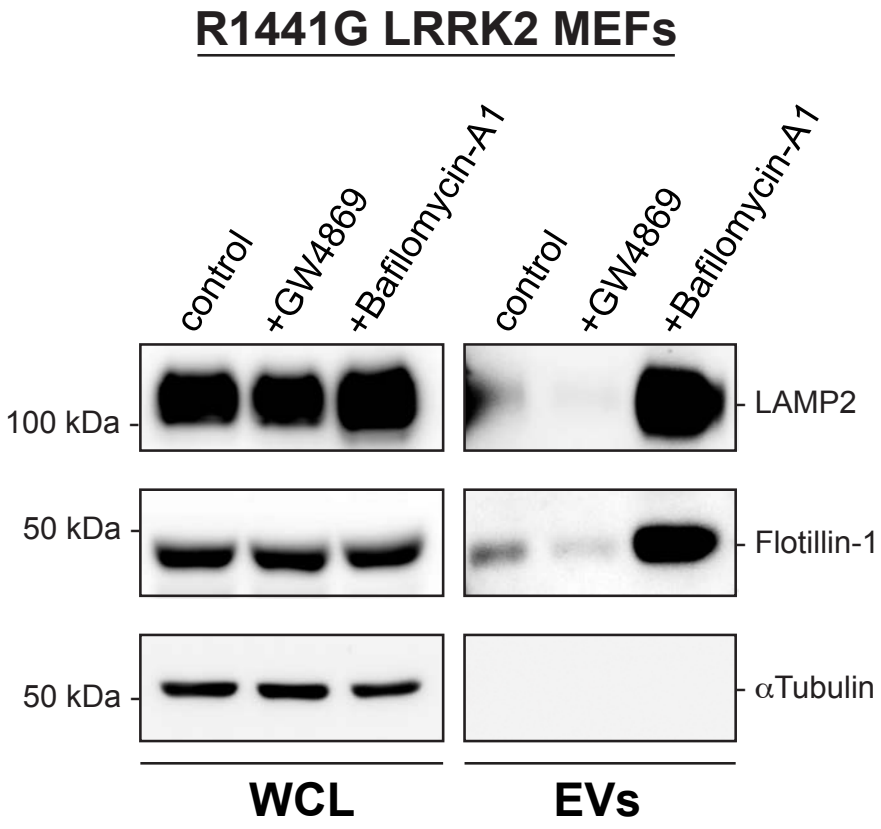
Supplemental Figure 3  Meneses-Salas et al.